JGR Atmospheres

RESEARCH ARTICLE
10.1029/2018JD030188

Comparison of Effective Radiative Forcing Calculations Using Multiple Methods, Drivers, and Models

T. Tang[1], D. Shindell[1], G. Faluvegi[2,3], G. Myhre[4], D. Olivié[5], A. Voulgarakis[6], M. Kasoar[6], T. Andrews[7], O. Boucher[8], P.M. Forster[9], Ø. Hodnebrog[4], T. Iversen[5], A. Kirkevåg[5], J.-F. Lamarque[10], T. Richardson[9], B.H. Samset[4], C.W. Stjern[4], T. Takemura[11], and C. Smith[9]

[1]Nicholas School of the Environment, Duke University, Durham, NC, USA, [2]Center for Climate System Research, Columbia University, New York, NY, USA, [3]NASA Goddard Institute for Space Studies, New York, NY, USA, [4]CICERO Center for International Climate and Environmental Research, Oslo, Norway, [5]Norwegian Meteorological Institute, Oslo, Norway, [6]Department of Physics, Imperial College London, London, UK, [7]Met Office Hadley Centre, Exeter, UK, [8]Institute Pierre-Simon Laplace, Sorbonne Université/CNRS, Paris, France, [9]Faculty of Environment, University of Leeds, Leeds, UK, [10]National Center for Atmospheric Research, Boulder, CO, USA, [11]Center for Oceanic and Atmospheric Research, Kyushu University, Fukuoka, Japan

Key Points:
- ERF estimated using fixed SST simulations and linear regression are fairly consistent for most climate forcings
- Multimodel mean ERF values vary by 10–50% with different methods, and this difference may reach 70–100% for black carbon
- Internal variability limits the application of linear regression technique in small-forcing experiments

Correspondence to:
T. Tang,
tao.tang@duke.edu

Citation:
Tang, T., Shindell, D., Faluvegi, G., Myhre, G., Olivié, D., Voulgarakis, A., et al. (2019). Comparison of effective radiative forcing calculations using multiple methods, drivers, and models. *Journal of Geophysical Research: Atmospheres*, *124*. https://doi.org/10.1029/2018JD030188

Received 18 DEC 2018
Accepted 26 MAR 2019
Accepted article online 2 APR 2019

Abstract We compare six methods of estimating effective radiative forcing (ERF) using a set of atmosphere-ocean general circulation models. This is the first multiforcing agent, multimodel evaluation of ERF values calculated using different methods. We demonstrate that previously reported apparent consistency between the ERF values derived from fixed sea surface temperature simulations and linear regression holds for most climate forcings, excluding black carbon (BC). When land adjustment is accounted for, however, the fixed sea surface temperature ERF values are generally 10–30% larger than ERFs derived using linear regression across all forcing agents, with a much larger (~70–100%) discrepancy for BC. Except for BC, this difference can be largely reduced by either using radiative kernel techniques or by exponential regression. Responses of clouds and their effects on shortwave radiation show the strongest variability in all experiments, limiting the application of regression-based ERF in small forcing simulations.

Plain Language Summary Climate drivers such as greenhouse gases and aerosols influence the Earth's climate by perturbing the Earth's energy budget at the top of the atmosphere, which is referred to as effective radiative forcing (ERF) when the atmospheric response is included in the calculation. ERF plays a crucial role in understanding the climate response to these drivers and predicting long-term climate change. Previously, ERFs have been estimated for greenhouse gases using two techniques that generally lead to similar values. Here we show that such consistency holds for most climate drivers. ERF values estimated from different methods may differ by 10–50%, and this difference may reach 70–100% for black carbon. Regression techniques do not work well in some models when imposed forcings are relatively small.

1. Introduction

Effective radiative forcing (ERF) is defined as the net downward radiative flux at the top of the atmosphere (TOA) after allowing for atmospheric temperature, water vapor, and clouds to adjust but with surface temperature or a portion of surface conditions unchanged (Myhre, Shindell, et al., 2013). It has been shown to be a more accurate indicator of the temperature response to forcing agents than the standard stratospherically adjusted radiative forcing, due to the inclusion of tropospheric adjustments. Better estimation of ERF is crucial to understanding the climate response to different forcings as well as predicting long-term climate change.

Two methods are commonly employed to determine ERF (see section 2): One is to simulate the climate response with fixed sea surface temperature (fsst) simulations (Hansen et al., 2002); the other is to linearly regress the net TOA radiative flux against global mean temperature change (ΔT) in a transient model simulation (Gregory et al., 2004). It has been reported that the values from these two methods are quantitatively consistent (Andrews et al., 2012). However, the ERF values from both methods may be biased. The former method allows land response in the simulations, and although Hansen et al. (2005) showed that accounting for land adjustment substantially increases ERF values, this is typically not included in fsst ERF calculations. The latter assumes a constant feedback parameter of the climate system in the adjustment process, which

Table 1
Descriptions of the Nine Precipitation Driver and Response Model Intercomparison Project Models Used in This Study

Model name	Version	Resolution	Ocean setup	Aerosol setup	References
CanESM	2010	2.8 × 2.8 (35 levels)	Coupled	Emission	Arora et al. (2011)
GISS-E2	E2-R	2 × 2.5 (40 levels)	Coupled	Fixed concentration	Schmidt et al. (2014)
HadGEM2-ES	6.6.3	1.875 × 1.25 (38 levels)	Coupled	Emissions	Collins et al. (2011)
HadGEM3	GA 4.0	1.875 × 1.25 85 levels	Coupled	Fixed concentration	Bellouin et al. (2011) and Walters et al. (2014)
MIROC-SPRINTARS	5.9.0	T85 (40 levels)	Coupled	HTAP2 emissions	Takemura et al. (2005), Takemura et al. (2009), and Watanabe et al. (2010)
CESM-CAM4	1.0.3	2.5 × 1.9 (26 levels)	Slab	Fixed concentration	Neale et al. (2010) and Gent et al. (2011)
CESM-CAM5	1.1.2	2.5 × 1.9 (30 levels)	Coupled	Emissions	Hurrell et al. (2013), Kay et al. (2015), and Otto-Bliesner et al. (2016)
NorESM	1-M	2.5 × 1.9 (26 levels)	Coupled	Fixed concentration	Bentsen et al. (2013), Iversen et al. (2013), and Kirkevåg et al. (2013)
IPSL-CM	5A	3.75 × 1.9 (19 levels)	Coupled	Fixed concentration	Dufresne et al. (2013)

Note. GA = Global Atmosphere; HTAP2 = Hemispheric Transport Air Pollution, Phase 2.

has been questioned by recent studies (Andrews et al., 2015; Armour et al., 2013; Gregory & Andrews, 2016; Proistosescu & Huybers, 2017). For example, Armour et al. (2013) suggest that the linear regression technique has fundamental biases because the slope depends on the regions where the surface is warming most rapidly at the time when the regression is performed. Andrews et al. (2015) suggest that the feedback parameters would become less negative after a few decades, making the response concave instead of linear and leading to ERF values that are low biased using linear regression. Thus, a better understanding of ERF estimated with different methods is needed. There is no study so far, to our best knowledge, that compares the ERF values estimated with different approaches and multiple climate drivers and models. This study aims to bridge this gap, comparing the effects of methodological choices on the estimation of ERF values, using a group of global climate models forced with five different climate drivers. Data and methods are described in section 2. Results are presented in section 3, and discussions and summary are given in section 4.

2. Data and Methods

2.1. Model Data

This study employs output from models participating in the Precipitation Driver and Response Model Intercomparison Project (PDRMIP), utilizing simulations examining the individual responses to CO_2, CH_4, solar insolation, black carbon (BC), and sulfate aerosols. The nine models used in this study are CanESM, GISS, HadGEM2, HadGEM3, MIROC, CAM4, CAM5, NorESM, and IPSL (see Table 1). In these simulations, global-scale perturbations were applied to the models: a doubling of CO_2 concentration ($CO_2 \times 2$), a tripling of CH_4 concentration ($CH_4 \times 3$), a 2% increase in solar irradiance (Solar + 2%), a tenfold increase of present-day BC concentration/emisssion (BC × 10), and a fivefold increase of present-day SO_4 concentration/emission ($SO_4 \times 5$). All perturbations were abrupt. Greenhouse gas and solar perturbations were applied relative to the models' baseline values. For aerosol perturbations, monthly year 2000 concentrations were derived from the AeroCom Phase II initiative (Myhre, Samset, et al., 2013) and multiplied by the stated factors in concentration-driven models. Some models were unable to perform simulations with prescribed concentrations. These models multiplied emissions by these factors instead, using either the same emissions or in one case another data set (Table 1). Each perturbation was run in two configurations, a 15-year fsst simulation and a 100-year coupled simulation. One model (CESM-CAM4) used a slab ocean setup for the coupled simulation, whereas the others used a full dynamic ocean. More detailed descriptions of PDRMIP and its initial findings are given in Samset et al. (2016), Myhre et al. (2017), and Tang et al. (2018).

2.2. Estimating ERF

For fsst simulations, ERF (ERF_fsst) is typically diagnosed by calculating the change of global mean TOA radiative flux (Hansen et al., 2002):

Table 2
Forcing, Feedback, and Global Mean Land Temperature Change (ΔT_land) for the $CO_2 \times 2$ Experiment

	$CO_2 \times 2$							
	ERF (W/m^2)							
Model	fsst	linr	fsst_ΔTland	poly	exp	kernel	$-\alpha$ ($W \cdot m^{-2} \cdot K^{-1}$)	ΔT_land (K)
CanESM	3.57	4.38	4.31	4.15	5.15	4.01	−1.37	0.46
GISS	4.06	4.32	6.50	2.85	4.95	4.59	−2.22	0.56
HadGEM2	3.35	3.22	4.08	4.26	3.97	3.92	−0.78	0.49
HadGEM3	3.65	3.52	4.36	3.69	3.98	4.28	−0.72	0.61
MIROC	3.62	4.13	5.22	4.41	5.43	4.02	−1.74	0.45
CAM4	3.62	3.04	4.36	3.64	6.39	4.07	−0.98	0.54
CAM5	4.08	4.09	5.55	3.05	4.68	4.63	−1.23	0.67
NorESM	3.50	3.25	4.34	5.54	4.31	3.82	−1.11	0.40
IPSL	3.39	3.09	4.28	3.64	3.47	3.80	−0.76	0.53
MMM ± 1std	3.65 ± 0.26	3.67 ± 0.55	4.78 ± 0.81	3.91 ± 0.80	4.70 ± 0.89	4.13 ± 0.31	−1.21 ± 0.50	0.52 ± 0.09

Note. 1 std indicates one standard deviation across the nine models. ERF = effective radiative forcing; fsst = fixed sea surface temperature.

$$\mathrm{ERF\_fsst} = \Delta\mathrm{SW} + \Delta\mathrm{LW}, \tag{1}$$

where ΔSW and ΔLW indicate the change of shortwave (SW) and longwave (LW) radiation at the TOA, respectively. For this calculation, we use years 6–15 from the fsst simulations. In ERF_fsst, the sea surface temperature and sea ice are fixed, while the land surface is allowed to adjust; as in practice, it is difficult to fix land temperature in the models. This means the global temperature has partially responded to the forcing, which causes the original external forcing to be underestimated. To account for this, Hansen et al. (2005) proposed a modified definition of ERF based on fsst simulations:

$$\mathrm{ERF\_fsst\_\ \Delta Tland} = \Delta\mathrm{SW} + \Delta\mathrm{LW} + \Delta\mathrm{T\_land}/\lambda, \tag{2}$$

where ΔT_land is the change in land surface air temperature and λ is the climate sensitivity parameter ($K \cdot W^{-1} \cdot m^{-2}$, in this case evaluated from the PDRMIP $CO_2 \times 2$ experiment). Like all ERFs, ERF_fsst_ΔTland allows tropospheric and stratospheric conditions to adjust to the presence of the forcing agent.

For regression, following Gregory et al. (2004), global mean radiative flux at the TOA is linearly regressed against ΔT in the coupled simulations to obtain ERF_linr:

$$\mathrm{N} = \mathrm{F}–\mathrm{H} = \mathrm{F}–\alpha\times\Delta\mathrm{T}, \tag{3}$$

where N is the net radiation flux (W/m^2, positive downward), F is the imposed forcing (W/m^2, positive downward), and H is the radiative response caused by the climate change (W/m^2, positive upward), which is linearly proportional to global surface temperature change (ΔT). All values in equation (3) are global averages (W/m^2). α is the climate feedback parameter ($W \cdot m^{-2} \cdot K^{-1}$), indicating the strength of the climate system's net feedback. If F and α are constant, N is a linear function of ΔT with a slope of $-\alpha$ and an intercept of F ($N = -\alpha \times \Delta T + F$). When $\Delta T = 0$, the intercept F = N, which is thus the ERF. Like ERFs diagnosed from fsst simulations, rapid adjustments of both the troposphere and stratosphere, including indirect effects of aerosols, are included. Note that although the ERF is a short-term concept (e.g., a few months after the forcing is imposed), the regression results inherently depend on the evolution of the climate system on longer time scales (e.g., a few decades; Gregory et al., 2004). The first 30-year of data were primarily used for regression analyses in this study.

We also apply two simple curved fits to the evolution of N and ΔT. The first is an exponential fit (ERF_exp):

$$\mathrm{N} = \mathrm{a}\times\exp\,(\mathrm{b}\times\Delta\mathrm{T}), \tag{4}$$

where a and b are the best-fit coefficients. When $\Delta T = 0$, N = a, which thus gives the ERF.

The second is a quadratic polynomial fit (ERF_poly):

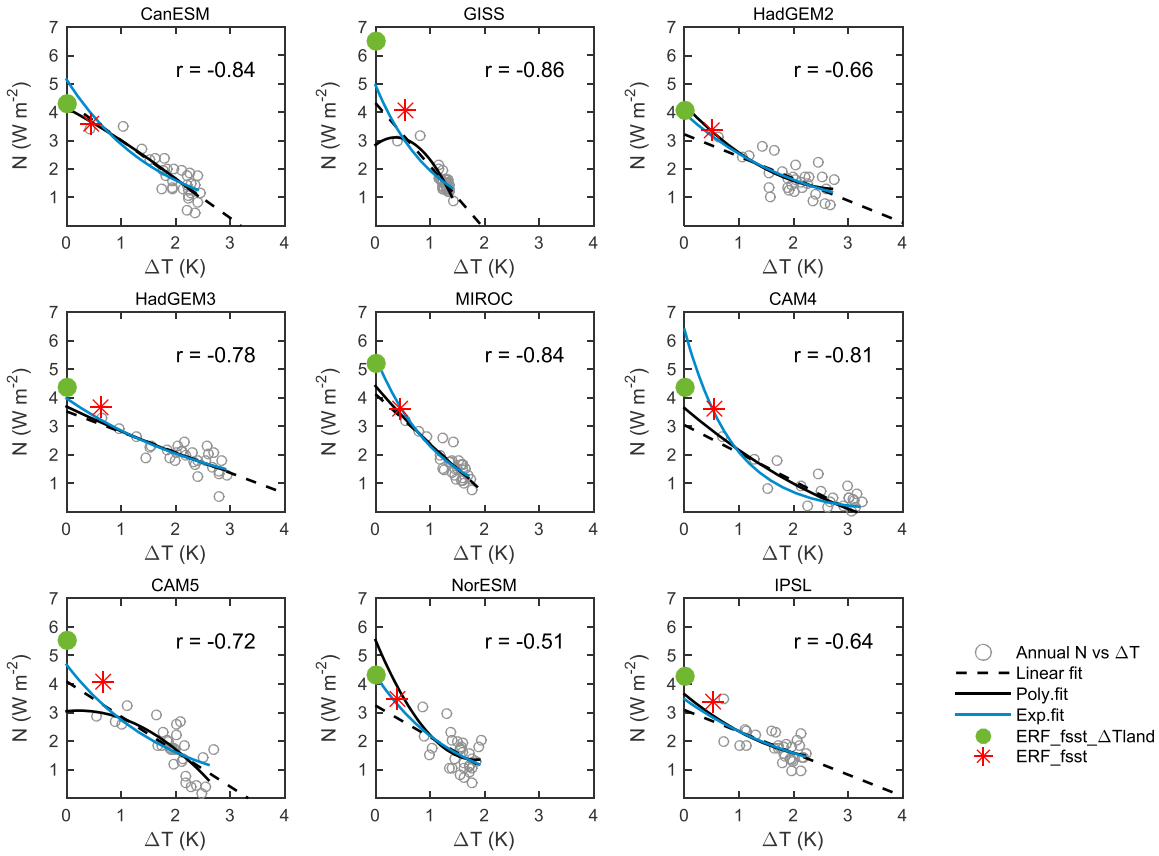

Figure 1. The evolution of radiative imbalance (N) with surface temperature change (ΔT) in the $CO_2 \times 2$ experiments, with a linear fit (black dashed line), a quadratic polynomial fit (black solid line), and an exponential fit (blue line). The intercepts of the fits indicate ERF_linr, ERF_poly, and ERF_exp, respectively. The *y* coordinates of green circles indicate ERF_fsst_ΔTland and red stars indicate ERF_fsst. The *x* coordinates of red stars indicate the global mean surface temperature change due to land (ΔT_land) in the fsst experiment. Linear correlation coefficients between N and ΔT are shown in the upper-right corners. ERF = effective radiative forcing; fsst = fixed sea surface temperature.

$$N = p1 \times \Delta T^2 + p2 \times \Delta T + p3, \tag{5}$$

where p1, p2, and p3 are the best-fit coefficients. When $\Delta T = 0$, $N = p3$, which is hence the ERF.

Another method evaluated in this study involves the technique of radiative kernels (Soden et al., 2008).

$$ERF\_kernel = ERF\_fsst - A_{T\_land} - A_T - A_q - A_a. \tag{6}$$

In this approach, the ERF_kernel value is obtained by subtracting the rapid adjustments associated with the land surface change from the ERF_fsst (obtained by equation (1)) while keeping rapid adjustments in the atmosphere that are not as directly associated with the land surface response, such as cloud responses. A_x are the rapid adjustments associated with land surface responses, which include land surface temperature (A_{T_land}) and albedo (A_a). In addition, land surface temperature change also causes changes in the tropospheric temperature (A_T), and here we assume a constant lapse rate in the troposphere, therefore the same change in tropospheric temperature as that of the surface. For water vapor, the fraction of the radiative flux change from a constant lapse rate to the full tropospheric temperature change has been used to scale the calculation of total water vapor change in order to account for the portion of water change associated with the surface temperature response (A_q). A rapid adjustment is the product of the direct radiative response to an incremental change in the respective variable and the total climate response of that variable. The former term is the radiative kernel, derived from a single offline radiative transfer model, while the latter is estimated from the response of a given PDRMIP model. More details of the radiative kernel method are given in Zhang and Huang (2014), Chung and Soden (2015), Myhre et al. (2018), and Smith et al. (2018).

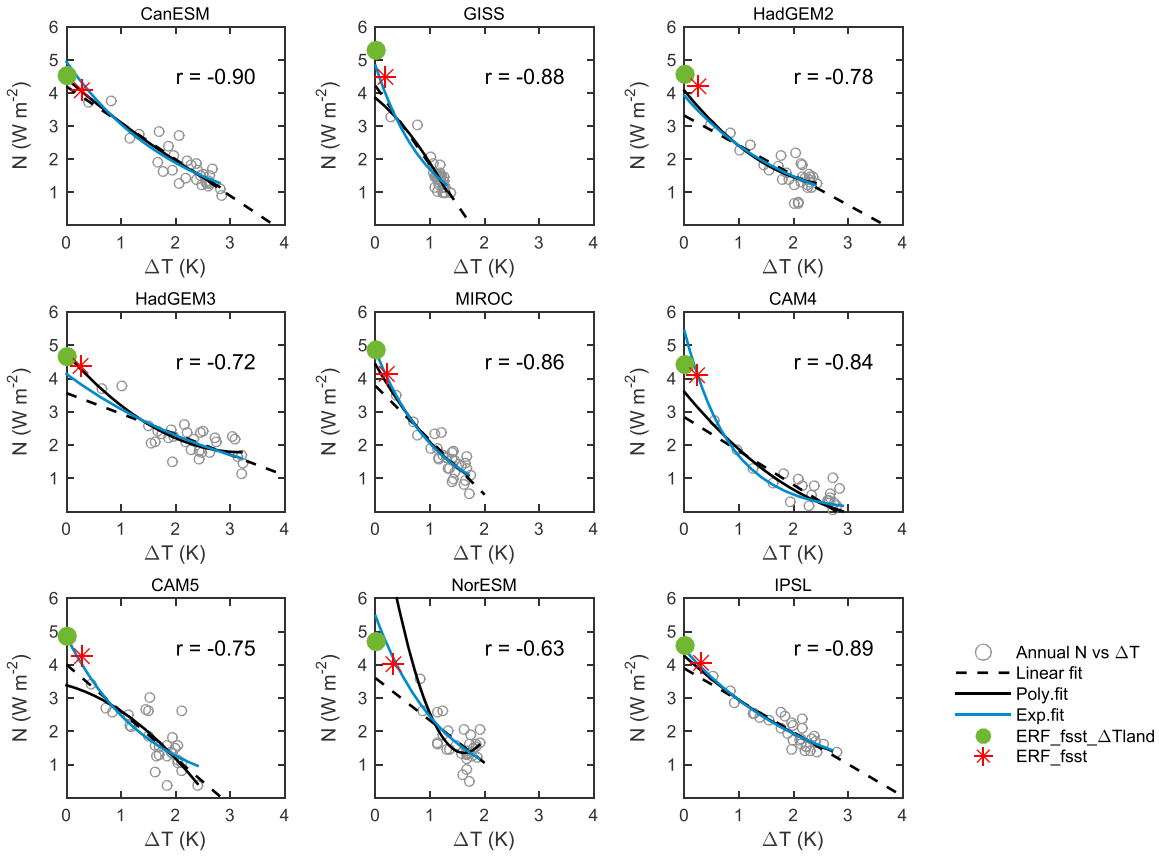

Figure 2. Same as Figure 1 but for Solar + 2% experiment.

Uncertainties are reported for multimodel mean (MMM) values based on the model-to-model variation in results. Additional discussion of uncertainties is presented in section 4.

3. Results

The results from the $CO_2 \times 2$ experiment for each model are shown in Table 2 and Figure 1. The MMM ERF_fsst is 3.65 ± 0.26 W/m^2 and ERF_linr is 3.67 ± 0.55 W/m^2. These are quantitatively consistent (Table 2), in line with Gregory et al. (2004) and Andrews et al. (2012). All models show fairly strong linear correlations between N and ΔT (Figure 1). Five models show larger values of ERF_fsst than ERF_linr and vice versa for the remaining models. The intermodel spread in ERF_linr is much larger than that of ERF_fsst, consistent with the results of Forster et al. (2016), which is presumably due to the extra processes involving the ocean in the coupled simulations and faster increase in the signal-to-noise ratio in equilibrium fsst simulations. When it comes to ERF_fsst_ΔTland, the MMM value is 4.78 W/m^2, which is roughly 30% larger than either ERF_fsst or ERF_linr, due to the inclusion of land adjustment in the case of comparison with ERF_fsst. The models with greater increases from ERF_fsst to ERF_fsst_ΔTland generally show stronger feedback (e.g., GISS and MIROC). Examining the two curved regression fits, MMM values are 3.91 W/m^2 for ERF_poly and 4.70 W/m^2 for ERF_exp, making the latter consistent with ERF_fsst_ΔTland, though large discrepancies occur in some individual models. Three models (CanESM, GISS, and CAM5) show opposite curvature in the polynomial fit relative to the exponential fit. We calculated the root mean square errors for all three regression methods, which give similar goodness of fit (Table 7). Thus, it is difficult to determine which one is better from a statistical perspective. The MMM of ERF_kernel is 4.13 W/m^2, which is roughly 13% larger than ERF_fsst but smaller than the ERF_fsst_ΔTland. This indicates that the sign of the net adjustments due to albedo, tropospheric temperatures, and tropospheric water vapor is opposite to that of the land surface temperature in a warming scenario.

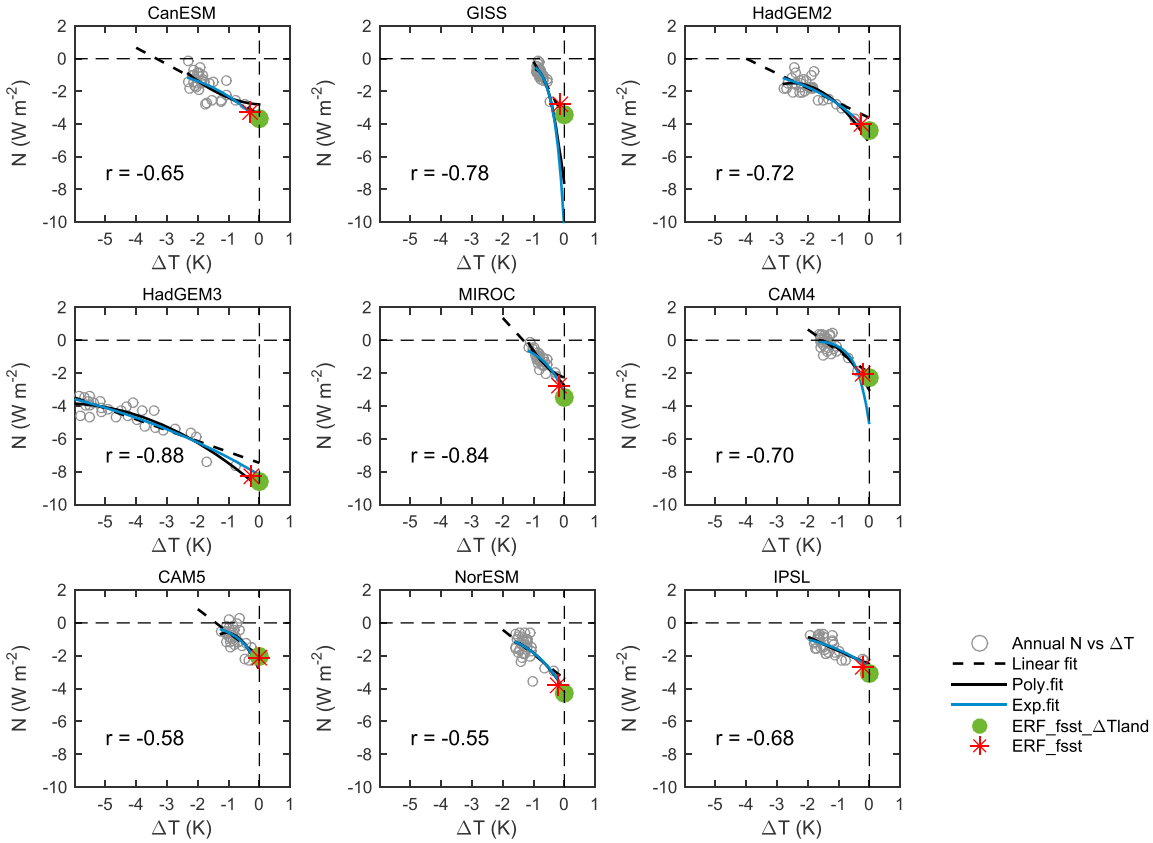

Figure 3. Same as Figure 1 but for $SO_4 \times 5$ experiment.

The results for the Solar + 2% and $SO_4 \times 5$ experiments are similar to the $CO_2 \times 2$ experiment (see Figures 2 and 3 and Tables 3 and 4). The magnitudes of the forcings are comparable to that of the $CO_2 \times 2$ experiment, with MMM values of 4.19 ± 0.15 and −3.52 ± 1.90 W/m^2 for the Solar + 2% and $SO_4 \times 5$ experiments (ERF_fsst), respectively. All nine models show significant linear correlations between N and ΔT, and the MMM values of ERF_linr and ERF_fsst are again consistent. For the Solar + 2% experiment, both ERF_poly and ERF_exp MMM values are consistent with ERF_fsst_ΔTland. For $SO_4 \times 5$ experiment, both ERF_poly and ERF_exp methods give larger MMM values than ERF_fsst_ΔTland, but they are within the uncertainty ranges. All three regression methods show similar goodness of fit (Table 7). However,

Table 3
Same as Table 2 but for Solar + 2% Experiment

Solar + 2%								
	ERF (W/m^2)							
Model	fsst	linr	fsst_ΔTland	poly	exp	kernel	−α (W·m^{-2}·K^{-1})	ΔT_land (K)
CanESM	4.09	4.20	4.53	4.44	4.95	4.24	−1.10	0.27
GISS	4.48	4.22	5.30	3.85	4.83	4.57	−2.40	0.19
HadGEM2	4.20	3.32	4.58	4.08	3.92	4.38	−0.90	0.26
HadGEM3	4.36	3.56	4.68	4.75	4.14	4.56	−0.62	0.27
MIROC	4.15	3.78	4.85	4.43	4.84	4.31	−1.63	0.20
CAM4	4.11	2.84	4.43	3.60	5.44	4.21	−1.02	0.24
CAM5	4.24	4.01	4.88	3.39	4.85	4.41	−1.41	0.29
NorESM	4.01	3.60	4.69	9.40	5.47	4.20	−1.27	0.32
IPSL	4.07	3.89	4.56	4.27	4.47	4.27	−0.96	0.30
MMM ± 1std	4.19 ± 0.15	3.71 ± 0.44	4.72 ± 0.26	4.70 ± 1.82	4.77 ± 0.52	4.35 ± 0.14	−1.26 ± 0.52	0.26 ± 0.05

Table 4
Same as Table 2 but for $SO_4 \times 5$ Experiment

$SO_4 \times 5$								
	ERF (W/m^2)						$-\alpha$ ($W \cdot m^{-2} \cdot K^{-1}$)	
Model	fsst	linr	fsst_ΔTland	poly	exp	kernel		ΔT_land (K)
CanESM	−3.24	−3.39	−3.71	−2.80	−3.85	−3.50	−1.01	−0.30
GISS	−2.79	−3.59	−3.46	−7.70	−10.50	−2.91	−3.41	−0.15
HadGEM2	−4.02	−3.63	−4.44	−5.17	−4.52	−4.26	−0.91	−0.28
HadGEM3	−8.26	−7.46	−8.56	−8.97	−8.20	−8.47	−0.66	−0.26
MIROC	−2.77	−2.75	−3.47	−2.27	−3.24	−2.82	−2.05	−0.19
CAM4	−2.04	−2.00	−2.31	−3.05	−5.14	−2.18	−1.33	−0.20
CAM5	−2.10	−2.02	−2.07	−2.90	−2.78	−2.02	−1.43	0.02
NorESM	−3.79	−3.40	−4.29	−4.06	−4.09	−3.90	−1.49	−0.24
IPSL	−2.70	−2.54	−3.09	−2.50	−2.69	−2.87	−0.84	−0.24
MMM ± 1std	−3.52 ± 1.90	−3.42 ± 1.64	−3.93 ± 1.91	−4.38 ± 2.43	−5.00 ± 2.65	−3.66 ± 1.95	−1.46 ± 0.84	−0.20 ± 0.09

polynomial fits show the opposite curvature in some individual models again. The MMM values using the ERF_kernel method are larger than ERF_fsst but smaller than ERF_fsst_ΔTland for both experiments. The feedback parameters remain essentially unchanged when compared with the $CO_2 \times 2$ experiment for all the models in both experiments.

The behavior is different, however, for the BC × 10 experiment (Table 5 and Figure 4). Despite the large perturbation (BC × 10), the forcing is small in some models, with a MMM value of 1.35 ± 0.98 W/m^2 (ERF_fsst), roughly one third of that for the $CO_2 \times 2$ experiment. The ERF_linr diverges more substantially from ERF_fsst. In fact, except for the CanESM, GISS, and IPSL models, the remaining six models show at least 25% smaller values in ERF_linr than ERF_fsst. There are only five models (CanESM, GISS, HadGEM2, MIROC, and CAM5) that show fairly good correlations ($r > 0.48$, this value is chosen because of the large gap between 0.49 and 0.33, see Figure 4) between N and ΔT, and the largest r is only 0.68, indicating that the relationship between N and ΔT is noisy. When only these five models are considered, ERF_linr is 30% smaller than ERF_fsst on average. ERF_fsst_ΔTland is 21% larger than ERF_fsst and 72% larger than ERF_linr, based on MMM values. Both ERF_poly and ERF_exp are less than ERF_fsst_ΔTland, and the ERF_kernel values are almost the same as ERF_fsst but 13% smaller than the ERF_fsst_ΔTland values on average. For all methods, the model-to-model variability is large, and so it is difficult to evaluate the robustness of differences between methodologies. For example, ERF_linr and ERF_fsst differ by up to a factor of two in several models, but they are very similar in others. The feedback parameters remain nearly unchanged in these five models relative to the simulations discussed previously.

Table 5
Same as Table 2 but for BC × 10 Experiment

BC × 10								
	ERF (W/m^2)						$-\alpha$ ($W \cdot m^{-2} \cdot K^{-1}$)	ΔT_land (K)
Model	fsst	linr	fsst_ΔTland	poly	exp	kernel		
CanESM*	1.55	1.57	1.96	1.59	2.01	1.65	−1.08	0.25
GISS*	1.23	1.06	1.57	1.07	1.91	1.32	−2.15	0.08
HadGEM2*	2.90	1.45	3.18	2.43	2.03	3.05	−0.66	0.19
HadGEM3	0.70	0.31	0.82	−0.02	0.30	0.75	−0.18	0.10
MIROC*	0.63	0.47	0.64	0.48	0.44	0.67	−1.72	0.00
CAM4	0.77	0.08	0.92	0.41	N/A	0.89	−0.14	0.11
CAM5*	0.42	0.22	0.82	0.23	0.14	0.40	−1.13	0.19
NorESM	1.41	1.04	1.75	2.94	2.32	1.53	−1.19	0.16
IPSL	0.82	0.69	0.93	0.80	0.76	0.87	−0.68	0.06
MMM ± 1std	1.35 ± 0.98	0.95 ± 0.59	1.63 ± 1.02	1.16 ± 0.89	1.31 ± 0.93	1.42 ± 1.04	−1.35 ± 0.59	0.14 ± 0.10

Note. N/A indicates the exponential fit gives an error. Models with linear fit correlations $|r| > 0.48$ (Figure 4) are denoted with an asterisk and multimodel mean calculations are based on these models only for all methods.

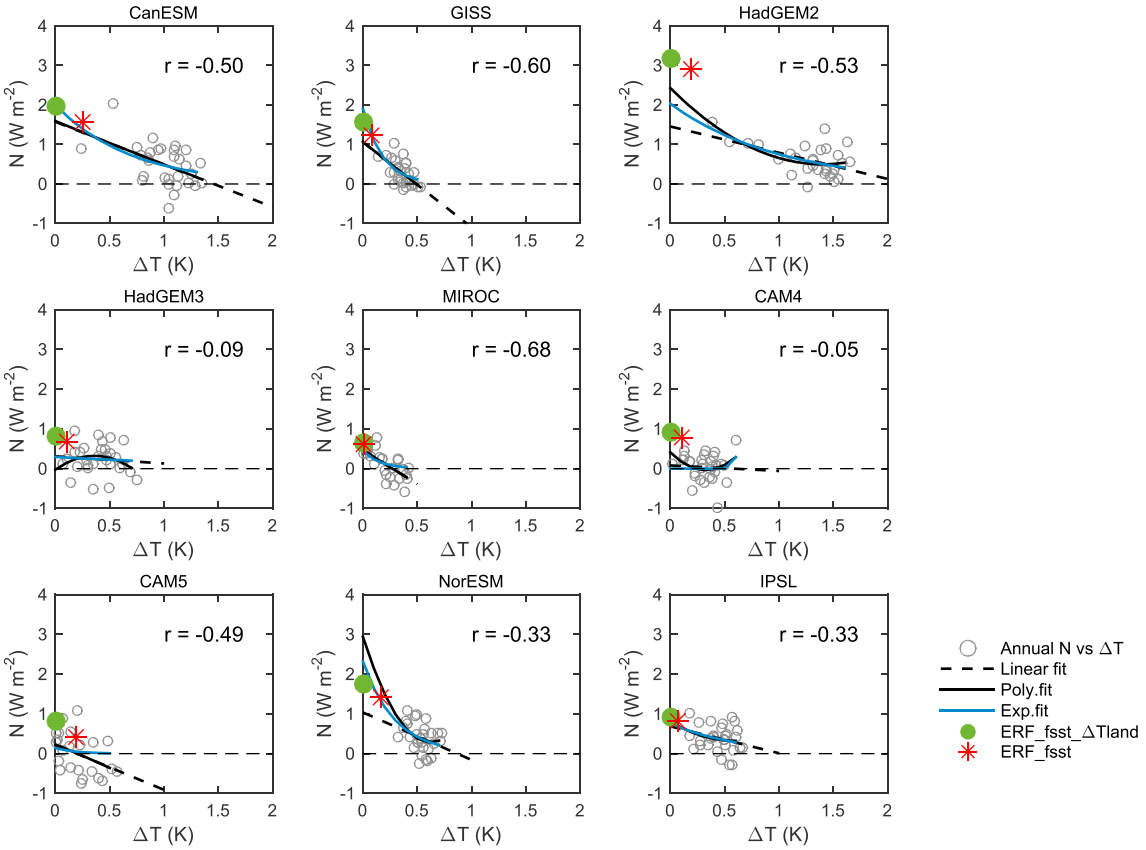

Figure 4. Same as Figure 1, but for BC × 10 experiment.

The results for the $CH_4 \times 3$ experiment (Table 6 and Figure 5) are somewhat similar to the BC × 10 experiment in that the climate forcing is relatively small (1.06 W/m^2 for MMM of ERF_fsst), and the linear regression technique does not work well for some models. Only four out of the nine models show fairly strong correlations between N and ΔT ($r >= 0.48$), with the largest r again being 0.68. When considering these four models only, however, the ERF_fsst (1.06 W/m^2) and ERF_linr (1.02 W/m^2) are consistent. ERF_fsst_ΔTland (1.38 W/m^2) is 30% larger than ERF_fsst, and ERF_exp (1.31 W/m^2) is consistent with ERF_fsst_ΔTland. These results are similar to those found for $CO_2 \times 2$. The ERF_poly (0.93 W/m^2),

Table 6
Same as Table 2 but for $CH_4 \times 3$ Experiment

$CH_4 \times 3$								
	ERF (W/m^2)							
Model	fsst	linr	fsst_ΔTland	poly	exp	kernel	−α (W·m^{-2}·K^{-1})	ΔT_land (K)
CanESM	1.36	0.89	1.65	0.79	0.88	1.46	−1.12	0.18
GISS*	1.34	1.45	2.02	0.89	1.45	1.60	−1.97	0.16
HadGEM2	0.97	0.55	1.05	0.93	0.59	1.03	−0.23	0.05
HadGEM3	1.39	1.15	1.56	1.62	1.43	1.49	−0.87	0.15
MIROC*	0.78	0.85	0.97	0.82	0.99	0.84	−1.60	0.05
CAM4*	1.27	0.80	1.45	1.13	1.86	1.36	−0.73	0.13
CAM5*	0.86	0.96	1.06	0.88	0.93	0.91	−1.77	0.09
NorESM	1.25	0.31	1.53	1.37	0.32	1.34	0.43	0.14
IPSL	1.58	1.32	1.88	1.75	1.45	1.75	−0.63	0.18
MMM ± 1std	1.06 ± 0.28	1.02 ± 0.30	1.38 ± 0.48	0.93 ± 0.14	1.31 ± 0.44	1.18 ± 0.36	−1.52 ± 0.55	0.11 ± 0.05

Note. Models with linear fit correlations $|r| \geq 0.48$ (Figure 5) are denoted with an asterisk and multimodel mean calculations are based on these models only for all methods.

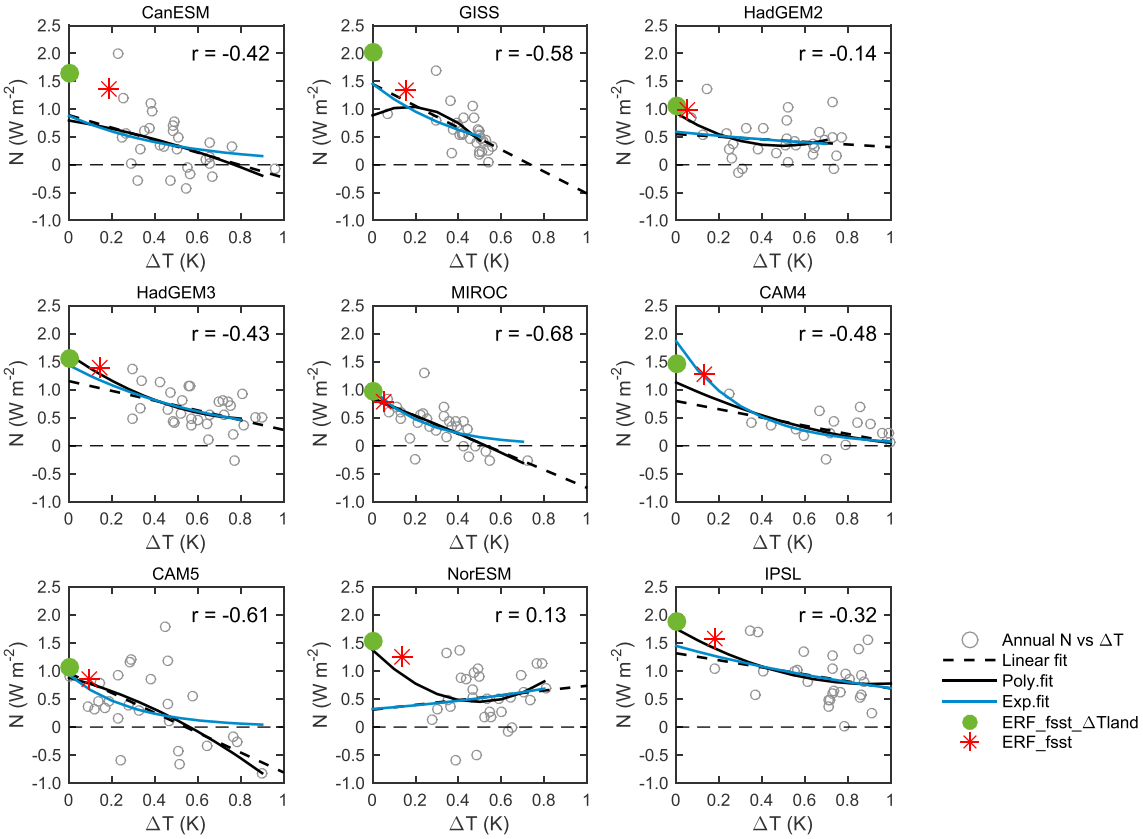

Figure 5. Same as Figure 1, but for the CH4 × 3 experiments.

however, is 32% lower than ERF_fsst_ΔTland and even lower than ERF_linr. The ERF_kernel again stands between ERF_fsst and ERF_fsst_ΔTland (Table 7).

4. Discussion and Summary

The magnitude of ERF_fsst_ΔTland, on average, is 32% (CO_2 × 2), 30% (CH_4 × 3), 13% (Solar + 2%), 21% (BC × 10), and 11% (SO_4 × 5) larger than ERF_fsst for the indicated experiments (Figure 6), due to the fact that the former accounts for land adjustment (ΔT_land / λ). In the greenhouse gas experiments, the adjustment to the forcing is roughly one third of the original ERF_fsst. Interestingly, ΔT_land in the CO_2 × 2 experiment is more than double that in the Solar + 2% and SO_4 × 5 experiments, despite their similar magnitude forcings. When compared with ERF_linr, ERF_fsst_ΔTland is also substantially larger. The MMM ratios of ERF_fsst_ΔTland/ERF_linr are 1.30, 1.35, 1.27, and 1.15 for the CO_2 × 2, CH_4 × 3, Solar + 2%, and SO_4 × 5 experiments, respectively. When it comes to BC, however, the ratio is 2.00 ± 1.04 (mean ± 1 standard deviation), obtained by calculating individual model ratios and then averaging them, which is much larger than the ratios in other experiments (Figure 6, blue bar). Note that this value is larger than the 72% reported above (Table 5) due to the different order of averaging; that value was obtained by taking the ratio of MMM values.

The consistency between MMM ERF_fsst and ERF_linr seen in prior work also holds in our current study across all experiments, except for BC (Figure 6, black bars). When land adjustment is included and values are hence presumably more physically realistic, however, the values derived from fsst simulations (ERF_fsst_ΔTland) are consistently larger

Table 7
Comparison of Multimodel Mean Values of Root-Mean-Squared Errors (in W/m^2), Which Shows the Goodness of the Fit

Experiment	Linear	Polynomial	Exponential
CO_2 × 2	0.42 ± 0.11	0.41 ± 0.11	0.43 ± 0.11
CH_4 × 3	0.37 ± 0.15	0.38 ± 0.16	0.40 ± 0.18
Solar + 2%	0.38 ± 0.11	0.36 ± 0.10	0.38 ± 0.11
BC × 10	0.36 ± 0.10	0.36 ± 0.11	0.37 ± 0.11
SO_4 × 5	0.45 ± 0.12	0.43 ± 0.12	0.44 ± 0.12

Note. For CH4 × 3 and BC × 10 experiments, only asterisked models (Tables 5 and 6) are used for multimodel mean calculations.

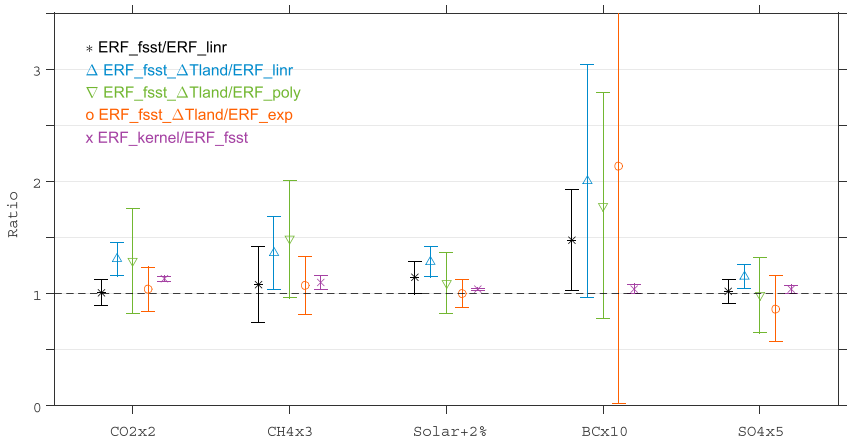

Figure 6. Comparison of different ERF values for each experiment. The symbols in each bar indicate multimodel mean values of ratios for each experiment, while the error bars show one standard deviation across the models. For $CH_4 \times 3$ and BC × 10 experiments, only the models with $|r| >= 0.48$ are used. ERF = effective radiative forcing; fsst = fixed sea surface temperature.

than ERF_linr. This can be plausibly attributed to time-varying feedback parameters leading to low biases in linear regressions (Andrews et al., 2015; Armour et al., 2013; Gregory & Andrews, 2016; Proistosescu & Huybers, 2017). To explore this further, we calculated the feedback parameters for land and ocean separately (by regressing N against global ΔT for each grid box) for all models and all experiments. The feedback parameters for years 1–30 are -1.14 ± 0.12 W·m^{-2}·K^{-1} over land and -1.33 ± 0.12 W·m^{-2}·K^{-1} over oceans, while for years 31–90, they are -0.49 ± 0.10 W·m^{-2}·K^{-1} over land and -0.68 ± 0.17 W·m^{-2}·K^{-1} over oceans. The feedback parameters thus become significantly less negative for both regions during the later years, but are similar in the two areas, with slightly larger values for the ocean. Thus, it is not clear that land feedbacks differ greatly from ocean feedbacks, although there is a very large spread across models (Table 8), but there is strong evidence that early feedbacks are larger than later ones. The two curved fits attempt to account for the concavity in feedbacks in the longer coupled runs. Based on MMM, the ERF values derived with a polynomial fit are consistent with the ERF_fsst_ΔTland in the Solar + 2% and $SO_4 \times 5$ experiments, but not in the other experiments (Figure 6, green bars), while the values using an exponential fit largely reconcile the regression results with the ERF_fsst_ΔTland values within the uncertainty range, with especially close correspondence for CO_2, CH_4, and solar experiments (Figure 6, red bars). For BC, the MMM ratio of ERF_fsst_ΔTland/ERF_exp remains high at 2.1 (Figure 6, red bar), though there is a large intermodel spread (mainly due to the CAM5 model). The reason for this

Table 8
Feedback Parameters for Land/Ocean in the Different Time Periods for the $CO_2 \times 2$ Experiment

	$CO_2 \times 2$					
	Years 1–30		Years 31–90		Years 1–90	
Model	Land	Ocean	Land	Ocean	Land	Ocean
CanESM	−1.49	−1.24	−1.21	−0.97	−1.30	−1.07
GISS	−2.62	−2.19	−1.42	−0.38	−2.40	−1.59
HadGEM2	−0.64	−0.86	−1.11	0.37	−0.81	−0.65
HadGEM3	−0.89	−0.56	−0.38	−0.21	−0.62	−0.26
MIROC	−1.20	−1.87	−1.14	−1.78	−1.22	−1.95
CAM4	−0.92	−0.88	0.27	0.25	−0.90	−0.82
CAM5	−0.57	−1.35	−0.38	−2.48	−0.89	−1.43
NorESM	−1.35	−0.94	0.18	−0.56	−0.85	−1.06
IPSL	−1.50	−0.45	−0.89	−0.31	−1.26	−0.52
MMM ± 1std	−1.24 ± 0.62	−1.15 ± 0.58	−0.68 ± 0.62	−0.67 ± 0.93	−1.14 ± 0.53	−1.04 ± 0.54

Note. The values in the text are multimodel mean for all five experiments.

Table 9
Comparison of Multimodel Mean (Mean ± 1 Standard Deviation) Values of ERF Derived With Different Time Periods

		ERF_linr		ERF_poly		ERF_exp	
Experiment	Year	ERF	RMSE	ERF	RMSE	ERF	RMSE
$CO_2 \times 2$	1–30	3.67 ± 0.55	0.42 ± 0.11	3.91 ± 0.80	0.41 ± 0.11	4.70 ± 0.89	0.43 ± 0.11
	1–100	3.45 ± 0.57	0.39 ± 0.09	4.12 ± 0.66	0.39 ± 0.09	5.30 ± 1.60	0.40 ± 0.10
$CH_4 \times 3$	1–30	1.02 ± 0.30	0.37 ± 0.15	0.93 ± 0.14	0.38 ± 0.16	1.31 ± 0.44	0.40 ± 0.18
	1–100	0.83 ± 0.18	0.37 ± 0.12	0.98 ± 0.23	0.36 ± 0.12	1.37 ± 0.79	0.38 ± 0.14
Solar + 2%	1–30	3.71 ± 0.44	0.38 ± 0.11	4.69 ± 1.82	0.36 ± 0.10	4.77 ± 0.52	0.38 ± 0.11
	1–100	3.45 ± 0.51	0.38 ± 0.08	4.41 ± 1.02	0.38 ± 0.08	5.06 ± 0.88	0.39 ± 0.09
BC × 10	1–30	0.95 ± 0.59	0.36 ± 0.10	1.16 ± 0.89	0.36 ± 0.11	1.31 ± 0.93	0.37 ± 0.11
	1–100	0.83 ± 0.52	0.38 ± 0.11	1.06 ± 0.73	0.38 ± 0.11	1.26 ± 0.98	0.40 ± 0.12
$SO_4 \times 5$	1–30	−3.42 ± 1.64	0.45 ± 0.12	−4.38 ± 2.43	0.43 ± 0.12	−5.00 ± 2.65	0.44 ± 0.12
	1–100	−3.06 ± 1.87	0.43 ± 0.10	−4.24 ± 1.91	0.42 ± 0.11	−4.91 ± 2.15	0.42 ± 0.11

discrepancy is not yet clear, though we reiterate that the regression-based results are highly uncertain in many models.

To further investigate uncertainties and the sensitivity to the time period used for the regression results, we compared the ERF values for three regressions using results from years 1–30 and years 1–100 of the coupled simulations (Table 9). In other studies, linear regressions have generally been applied to the first 20–30 years of data. Results based on shorter time spans (e.g., 10 years) would be subject to strong internal variability (Hansen et al., 2005). For ERF_poly and ERF_exp, there are no significant changes when more years are included except for the $CO_2 \times 2$ experiment, which shows a slight increase in both values, but they remain within the uncertainty ranges. For ERF_linr, however, there are systematic decreases (6–10%) across all five experiments when a longer time span is used due to time-varying feedback parameters. This analysis indicates that both ERF_poly and ERF_exp are less sensitive to the chosen time period. Moreover, all three regressions show similar goodness of fit.

For comparison, we also calculated the uncertainty ranges for the nonregression ERF values. For ERF_fsst, the MMM values are ±0.16 W/m^2 ($CO_2 \times 2$), ±0.17 W/m^2 ($CH_4 \times 3$), ±0.18 W/m^2 (Solar+2%), ±0.16 W/m^2 (BC × 10), and ±0.19 W/m^2 ($SO_4 \times 5$), based on the interannual variability of radiative fluxes. These uncertainty ranges are generally 0.12 W/m^2 larger in magnitude for the ERF_fsst_ΔTland due to the additional variability in climate sensitivity and land response (ΔTland). For ERF_kernel, the uncertainty in the additional kernel-derived adjustments was estimated by analyzing the spread in rapid adjustments calculated using six kernels from Smith et al. (2018) for each model. The spread in the rapid adjustments are generally 0.02–0.05 W/m^2 across most of the models and experiments. When combined with uncertainties of ERF_fsst, they produce MMM uncertainties (estimated by δERF_kernel = (δERF_fsst^2 + δrapid adjustments^2)$^{1/2}$, where δ is the uncertainty for each component) of ±0.17 W/m^2 ($CO_2 \times 2$), ±0.17 W/m^2 ($CH_4 \times 3$), ±0.19 W/m^2 (Solar + 2%), ±0.18 W/m^2 (BC × 10), and ±0.19 W/m^2 ($SO_4 \times 5$), similar to those of ERF_fsst and smaller than the regression-based analyses (Table 8).

Our analyses show that the ERF values may differ by ~10–50% with different methods, based on MMM results, and this difference may reach 100% for BC. It is difficult to determine, however, which method for calculating ERF is the best. Researchers need to choose the appropriate approach, depending on available model output, computation resources, and research needs. With fsst simulations, it is easy and fast to obtain either ERF_fsst or ERF_fsst_ΔTland values. However, for researchers who only have coupled simulations, regression methods are the only option to obtain the ERF. Linear regression is simple and is the most widely used (Myhre, Shindell, et al., 2013) and is also generally consistent with ERF_fsst values. The latter, however, neglects a known process (land temperature adjustment), and so arguably, ERF_fsst_ΔTland is a more physically realistic method. Based on MMM values, an exponential fit is shown to be more consistent with ERF_fsst_ΔTland values, though exceptions exist in individual models. In addition, it is less sensitive to the chosen time period than linear regression. The polynomial fit is sensitive to natural variability and may give opposite curvature to that inferred from a direct analysis of the feedback's temporal evolution (e.g., GISS model in Figure 1). We also investigated higher-order polynomial fits, but the curvatures do not fit the

evolution of N and ΔT. The radiative kernel method provides another option to obtain ERF values accounting for land-related responses and leads to only slight increases (4–13%) compared with ERF_fsst (Figure 6, purple bars). The disadvantage of this method is that it requires more output from the simulations and more computation resources compared with other approaches.

The poor correlations between N and ΔT for the BC × 10 experiments suggest that the regression technique may not work well in the BC × 10 experiment, at least for some models and for the time scales considered in this study. This may be partly attributable to internal variability. The forcing in the BC × 10 experiment is relatively small compared with the CO_2 × 2 experiment, ranging from 0.8–2.0 W/m^2 for most models. However, the interannual variability of N in the BC × 10 experiment ranges from 0.3–0.5 W/m^2, which is a substantial fraction of the forcing. Such variability blurs the relation of N and ΔT. Further analyses indicate that this variability is mainly associated with SW cloud effects (not shown), suggesting the pivotal role of low-level clouds on the unforced fluctuations of radiation budgets. Due to the larger forcing in CO_2 × 2, Solar + 2%, and SO_4 × 5 experiments (~ 4 W/m^2), the SW cloud effects did not significantly affect the fits in those cases, whereas the regression techniques do not work well for some models in the CH_4 × 3 and BC × 10 experiments with small forcing. Therefore, the regression techniques (linear, polynomial, and exponential) appear useful in those large-forcing experiments but should be used with caution in small-forcing simulations.

In this study, we compared six methods for estimating ERF values from nine models participating in the PDRMIP project. The consistency between the values of ERF_fsst and ERF_linr in prior studies holds for most climate forcings, except for BC. When land response is accounted for in fsst simulations, the ERF_fsst_ΔTland is roughly 10–30% larger than ERF_linr, however, and 100% larger for the BC × 10 experiments. Such adjustments can also be accounted for by using radiative kernels, which typically leads to values in between the ERF_fsst and ERF_fsst_ΔTland results. There is a tendency for the values derived from linear regression to be lower than ERF_fsst_ΔTland values, which appears to be explained by the time-varying feedbacks. Such differences can be largely eliminated by using an exponential regression, making them consistent with the fsst values with land adjustment included under most climate forcings based on MMM results. BC forcing is quite sensitive to the method used, the reasons for which merit further study.

Acknowledgments
We would like to acknowledge the helpful and constructive reviews that improved earlier version of this manuscript. The PDRMIP model output used in this study are available to public through the Norwegian NORSTORE data storage facility. We acknowledge the NASA High-End Computing Program through the NASA Center for Climate Simulation at Goddard Space Flight Center for computational resources to run the GISS-E2R model and support from NASA GISS. PDRMIP is partly funded through the Norwegian Research Council project NAPEX (project 229778). O. Boucher acknowledges HPC resources from CCRT under the gencmip6 allocation provided by GENCI (Grand Equipement National de Calcul Intensif). P. Forster and T. Richardson are supported by NERC grants NE/K007483/1 and NE/N006038/1. Ø. Hodnebrog was partly funded through the Norwegian Research Council project HYPRE (project 243942). A. Voulgarakis and M. Kasoar are supported by NERC under grant NE/K500872/1. HadGEM3-GA4 simulations used the MONSooN system supplied under the Joint Weather and Climate Research Programme of the Met Office and NERC. D. Olivié, A. Kirkevåg, and T. Iversen were supported by the Norwegian Research Council through the projects EVA (grant 229771), EarthClim (207711/E10), NOTUR (nn2345k), and NorStore (ns2345k). T. Takemura was supported by the supercomputer system of the National Institute for Environmental Studies, Japan, the Environment Research and Technology Development Fund (S-12-3) of the Ministry of the Environment, Japan and JSPS KAKENHI grant 15H01728 and 15 K12190. Computing resources for CESM1-CAM5 (ark:/85065/d7wd3xhc) simulations were provided by the Climate Simulation Laboratory at NCAR Computational and Information System Laboratory, sponsored by the National Science Foundation and other agencies.

References

Andrews, T., Gregory, J. M., & Webb, M. J. (2015). The dependence of radiative forcing and feedback on evolving patterns of surface temperature change in climate models. *Journal of Climate*, *28*(4), 1630–1648. https://doi.org/10.1175/JCLI-D-14-00545.1

Andrews, T., Gregory, J. M., Webb, M. J., & Taylor, K. E. (2012). Forcing, feedbacks and climate sensitivity in CMIP5 coupled atmosphere-ocean climate models. *Geophysical Research Letters*, *39*, L09712. https://doi.org/10.1029/2012GL051607

Armour, K. C., Bitz, C. M., & Roe, G. H. (2013). Time-varying climate sensitivity from regional feedbacks. *Journal of Climate*, *26*(13), 4518–4534. https://doi.org/10.1175/JCLI-D-12-00544.1

Arora, V. K., Scinocca, J. F., Boer, G. J., Christian, J. R., Denman, K. L., Flato, G. M., et al. (2011). Carbon emission limits required to satisfy future representative concentration pathways of greenhouse gases. *Geophysical Research Letters*, *38*, L05805. https://doi.org/10.1029/2010GL046270

Bellouin, N., Rae, J., Jones, A., Johnson, C., Haywood, J., & Boucher, O. (2011). Aerosol forcing in the Climate Model Intercomparison Project (CMIP5) simulations by HadGEM2-ES and the role of ammonium nitrate. *Journal of Geophysical Research*, *116*, D20206. https://doi.org/10.1029/2011JD016074

Bentsen, M., Bethke, I., Debernard, J. B., Iversen, T., Kirkevåg, A., Seland, Ø., et al. (2013). The Norwegian Earth System Model, NorESM1-M—Part 1: Description and basic evaluation of the physical climate. *Geoscientific Model Development*, *6*(3), 687–720. https://doi.org/10.5194/gmd-6-687-2013

Chung, E. S., & Soden, B. J. (2015). An assessment of direct radiative forcing, radiative adjustments, and radiative feedbacks in coupled ocean–atmosphere models. *Journal of Climate*, *28*(10), 4152–4170. https://doi.org/10.1175/JCLI-D-14-00436.1

Collins, W. J., Bellouin, N., Doutriaux-Boucher, M., Gedney, N., Halloran, P., Hinton, T., et al. (2011). Development and evaluation of an earth-system model–HadGEM2. *Geoscientific Model Development*, *4*(4), 1051–1075. https://doi.org/10.5194/gmd-4-1051-2011

Dufresne, J.-L., Foujols, M.-A., Denvil, S., Caubel, A., Marti, O., Aumont, O., et al. (2013). Climate change projections using the IPSL-CM5 earth system model: From CMIP3 to CMIP5. *Climate Dynamics*, *40*(9–10), 2123–2165. https://doi.org/10.1007/s00382-012-1636-1

Forster, P. M., Richardson, T., Maycock, A. C., Smith, C. J., Samset, B. H., Myhre, G., et al. (2016). Recommendations for diagnosing effective radiative forcing from climate models for CMIP6. *Journal of Geophysical Research: Atmospheres*, *121*, 12,460–12,475. https://doi.org/10.1002/2016JD025320

Gent, P. R., Danabasoglu, G., Donner, L. J., Holland, M. M., Hunke, E. C., Jayne, S. R., et al. (2011). The Community Climate System Model version 4. *Journal of Climate*, *24*(19), 4973–4991. https://doi.org/10.1175/2011JCLI4083.1

Gregory, J., Ingram, W., Palmer, M., Jones, G., Stott, P., Thorpe, R., et al. (2004). A new method for diagnosing radiative forcing and climate sensitivity. *Geophysical Research Letters*, *31*, L03205. https://doi.org/10.1029/2003GL018747

Gregory, J. M., & Andrews, T. (2016). Variation in climate sensitivity and feedback parameters during the historical period. *Geophysical Research Letters*, *43*, 3911–3920. https://doi.org/10.1002/2016GL068406

Hansen, J., Sato, M., Nazarenko, L., Ruedy, R., Lacis, A., Koch, D., et al. (2002). Climate forcings in Goddard Institute for Space Studies SI2000 simulations. *Journal of Geophysical Research*, (D18), 107, 4347. https://doi.org/10.1029/2001JD001143

Hansen, J., Sato, M., Ruedy, R., Nazarenko, L., Lacis, A., Schmidt, G., et al. (2005). Efficacy of climate forcings. *Journal of Geophysical Research*, 110, D18104. https://doi.org/10.1029/2005JD005776

Hurrell, J. W., Holland, M. M., Gent, P. R., Ghan, S., Kay, J. E., Kushner, P. J., et al. (2013). The Community Earth System Model: A framework for collaborative research. *Bulletin of the American Meteorological Society*, *94*(9), 1339–1360. https://doi.org/10.1175/BAMS-D-12-00121.1

Iversen, T., Bentsen, M., Bethke, I., Debernard, J., Kirkevåg, A., Seland, Ø., et al. (2013). The Norwegian Earth System Model, NorESM1-M—Part 2: Climate response and scenario projections. *Geoscientific Model Development*, *6*(2), 389–415. https://doi.org/10.5194/gmd-6-389-2013

Kay, J. E., Deser, C., Phillips, A., Mai, A., Hannay, C., Strand, G., et al. (2015). The Community Earth System Model (CESM) large ensemble project: A community resource for studying climate change in the presence of internal climate variability. *Bulletin of the American Meteorological Society*, *96*(8), 1333–1349. https://doi.org/10.1175/BAMS-D-13-00255.1

Kirkevåg, A., Iversen, T., Seland, Ø., Hoose, C., Kristjánsson, J. E., Struthers, H., et al. (2013). Aerosol–climate interactions in the Norwegian Earth System Model–NorESM1-M. *Geoscientific Model Development*, *6*(1), 207–244. https://doi.org/10.5194/gmd-6-207-2013

Myhre, G., Forster, P. M., Samset, B. H., Hodnebrog, Ø., Sillmann, J., Aalbergsjø, S. G., et al. (2017). PDRMIP: A Precipitation Driver and Response Model Intercomparison Project, protocol and preliminary results. *Bulletin of the American Meteorological Society*, *98*(6), 1185–1198. https://doi.org/10.1175/BAMS-D-16-0019.1

Myhre, G., Kramer, R. J., Smith, C. J., Hodnebrog, Ø., Forster, P., Soden, B. J., et al. (2018). Quantifying the importance of rapid adjustments for global precipitation changes. *Geophysical Research Letters*, *45*, 11,399–11,405. https://doi.org/10.1029/2018GL079474

Myhre, G., Samset, B. H., Schulz, M., Balkanski, Y., Bauer, S., Berntsen, T. K., et al. (2013). Radiative forcing of the direct aerosol effect from aerocom phase ii simulations. *Atmospheric Chemistry and Physics*, *13*(4), 1853–1877. https://doi.org/10.5194/acp-13-1853-2013

Myhre, G., Shindell, D., Bréon, F.-M., Collins, W., Fuglestvedt, J., Huang, J., et al. (2013). Anthropogenic and natural radiative forcing. In T. F. Stoker, D. Qin, G.-K. Plattner, M. Tignor, S. K. Allen, et al. (Eds.), *Climate change 2013: The physical science basis. Contribution of Working Group I to the Fifth Assessment Report of the Intergovernmental Panel on Climate Change* (pp. 659–740). Cambridge, UK and New York: Cambridge University Press.

Neale, R. B., Richter, J. H., Conley, A. J., Park, S., Lauritzen, P. H., Gettelman, A., et al. (2010). Description of the NCAR Community Atmosphere Model (cam 4.0). Boulder, CO.

Otto-Bliesner, B. L., Brady, E. C., Fasullo, J., Jahn, A., Landrum, L., Stevenson, S., et al. (2016). Climate variability and change since 850 CE: An ensemble approach with the Community Earth System Model. *Bulletin of the American Meteorological Society*, *97*(5), 735–754. https://doi.org/10.1175/BAMS-D-14-00233.1

Proistosescu, C., & Huybers, P. J. (2017). Slow climate mode reconciles historical and model-based estimates of climate sensitivity. *Science Advances*, *3*(7), e1602821. https://doi.org/10.1126/sciadv.1602821

Samset, B. H., Myhre, G., Forster, P. M., Hodnebrog, Ø., Andrews, T., Faluvegi, G., et al. (2016). Fast and slow precipitation responses to individual climate forcers: A PDRMIP multimodel study. *Geophysical Research Letters*, *43*, 2782–2791. https://doi.org/10.1002/2016GL068064

Schmidt, G. A., Kelley, M., Nazarenko, L., Ruedy, R., Russell, G. L., Aleinov, I., et al. (2014). Configuration and assessment of the GISS model-E2 contributions to the CMIP5 archive. *Journal of Advances in Modeling Earth Systems*, *6*, 141–184. https://doi.org/10.1002/2013MS000265

Smith, C. J., Kramer, R. J., Myhre, G., Forster, P. M., Soden, B. J., Andrews, T., et al. (2018). Understanding rapid adjustments to diverse forcing agents. *Geophysical Research Letters*, *45*, 12,023–12,031. https://doi.org/10.1029/2018GL079826

Soden, B. J., Held, I. M., Colman, R., Shell, K. M., Kiehl, J. T., & Shields, C. A. (2008). Quantifying climate feedbacks using radiative kernels. *Journal of Climate*, *21*(14), 3504–3520. https://doi.org/10.1175/2007JCLI2110.1

Takemura, T., Egashira, M., Matsuzawa, K., Ichijo, H., O'ishi, R., & Abe-Ouchi, A. (2009). A simulation of the global distribution and radiative forcing of soil dust aerosols at the last glacial maximum. *Atmospheric Chemistry and Physics*, *9*(9), 3061–3073. https://doi.org/10.5194/acp-9-3061-2009

Takemura, T., Nozawa, T., Emori, S., Nakajima, T. Y., & Nakajima, T. (2005). Simulation of climate response to aerosol direct and indirect effects with aerosol transport-radiation model. *Journal of Geophysical Research*, 110, D02202. https://doi.org/10.1029/2004JD005029

Tang, T., Shindell, D., Samset, B. H., Boucher, O., Forster, P. M., Hodnebrog, Ø., et al. (2018). Dynamical response of Mediterranean precipitation to greenhouse gases and aerosols. *Atmospheric Chemistry and Physics*, *18*(11), 8439–8452. https://doi.org/10.5194/acp-18-8439-2018

Walters, D. N., Williams, K. D., Boutle, I. A., Bushell, A. C., Edwards, J. M., Field, P. R., et al. (2014). The Met office unified model global atmosphere 4.0 and jules global land 4.0 configurations. *Geoscientific Model Development*, *7*(1), 361–386. https://doi.org/10.5194/gmd-7-361-2014

Watanabe, M., Suzuki, T., O'ishi, R., Komuro, Y., Watanabe, S., Emori, S., et al. (2010). Improved climate simulation by MIROC5: Mean states, variability, and climate sensitivity. *Journal of Climate*, *23*(23), 6312–6335. https://doi.org/10.1175/2010JCLI3679.1

Zhang, M., & Huang, Y. (2014). Radiative forcing of quadrupling CO_2. *Journal of Climate*, *27*(7), 2496–2508. https://doi.org/10.1175/JCLI-D-13-00535.1